



# Drought Monitoring and Response System: A Comparative Assessment of Machine Learning and Artificial Neural Network Approaches Using Remotely Sensed and Meteorological Data

Devansh Rao <sup>1</sup>, Nikhil Bhasin <sup>2</sup>, Ishita Menon <sup>2</sup>

<sup>1</sup> National Institute of Technology Trichy (NIT Trichy), Tamil Nadu, India

<sup>2</sup> Indian Institute of Science (IISc), Bengaluru, India.

## Abstract

Water, the universal solvent, is crucial for life, yet its preservation faces growing challenges from climate change and population growth. Understanding factors contributing to extreme events like droughts is vital for effective risk management. Drought inflicts substantial harm across social, economic, and agricultural domains, making an effective early warning and monitoring system essential, particularly given significant climatic variations and the anticipated increase in water scarcity and drought frequency. This study focuses on developing a resilient agricultural drought assessment system for Shandong province, China, using the three-month Standardized Precipitation Evapotranspiration Index (SPEI-3) as the reference variable. We used multi-source remote sensing and modeled data, including precipitation, soil moisture, vegetation indices (NDVI, EVI), and temperature, as input factors for three machine learning models: Bias-Corrected Random Forest (BRF), Extreme Gradient Boosting (XGBoost), and Support Vector Machines (SVM).

The results show that the BRF model significantly outperforms both SVM and XGBoost in simulating SPEI-3 values, achieving a high prediction accuracy (R-squared of 0.94) and a small prediction error (RMSE of 0.22) on the test set. Model stability, assessed through multiple runs and a leave-one-station-out cross-validation, further confirmed BRF's superior and more stable performance. An analysis of factor importance via the BRF model indicated that three-month cumulative precipitation is the most important factor in agricultural drought assessment, accounting for 55.17% of the relative importance, followed by soil moisture (10.2%). This research successfully validates the BRF model's high accuracy and stability for mapping the SPEI-3 index across space, offering a robust methodology for enhanced drought monitoring and response.

**Keywords:** Drought monitoring, Machine learning, Bias-Corrected Random Forest (BRF), Remote sensing, Standardized Precipitation Evapotranspiration Index (SPEI), Agricultural drought, Shandong Province, Climate variability

## INTRODUCTION

Drought is characterized by a temporary disruption in the balance of water resources caused by consistently lower-than-average rainfall. Its adverse effects on agriculture, economy, recreation, hydropower generation, and ecosystems are substantial. Droughts have the potential to result in crop failure, giving rise to significant challenges in food security and economic losses. Additionally, they diminish water reservoirs like lakes and rivers, impacting water distribution and energy supply directly. Furthermore, droughts can elevate plant mortality rates, trigger ecosystem fires, and compromise the capacity of vegetation to absorb carbon. Consequently, these factors contribute to the disruption of land carbon storage and its potential for storage. To comprehend drought and facilitate its monitoring and prediction, it is imperative to conduct in-depth studies on precipitation, soil conditions, vegetation, and their interconnected parameters. Drought indices have been developed worldwide to assess the initiation, severity, and geographical extent of droughts across meteorological, hydrological, and agricultural domains. These indices encompass various parameters, including precipitation, runoff, soil water storage, satellite-derived vegetation metrics, and land surface temperature. To comprehend the process and consequences of drought, it is essential to recognize key aspects such as intensity, duration, and spatial extent. The primary challenge in monitoring and analyzing drought lies in selecting appropriate indicators. Drought indices predominantly rely on the calculation of either individual or combined variables affected by drought to represent diverse drought characteristics. Consequently, over 160 drought indices have been developed by researchers, each possessing distinct advantages and limitations that warrant careful consideration. These indices fall into two categories: those based on meteorological observations and those based on remotely sensed observations. Meteorological drought indices, derived from ground-based measurements, utilize variables like precipitation and temperature, enabling precise monitoring of drought conditions in the vicinity of climate stations. Among them, the standard precipitation evapotranspiration index (SPEI) stands out as it incorporates both precipitation and temperature in its computation. Remote sensing provides continuous, comprehensive information on drought

conditions in both time and space, surpassing ground-based observations. Researchers use various sensors to calculate drought indices, including normalized difference vegetation index (NDVI) and enhanced vegetation index (EVI), for monitoring meteorological and agricultural drought. Advanced remote sensing products have spawned additional indices like soil moisture condition index (SMCI) and precipitation condition index (PCI) based on precipitation, temperature, evapotranspiration, and soil moisture. Despite capturing detailed spatial characteristics, remote sensing indices have limitations due to short observation times and challenges related to retrieval algorithms and atmospheric conditions.

Researchers have experimented with various models to enhance drought monitoring. Initially, they relied on stochastic models like the autoregressive integrated moving average model (ARIMA) to forecast drought, which could capture seasonality and time series lags. However, drought's essence being nonlinear, subsequent studies explored three types of models: physical, data-driven, and hybrid. Data-driven models, particularly artificial neural networks (ANN), have gained prominence due to their ability to improve prediction accuracy over physically-based models. Despite ANN's effectiveness in short and long-term predictions, it struggles with non-stationarity in drought estimation due to time series lags. Consequently, interest has surged in employing machine learning approaches, especially as more advanced methods have emerged, demonstrating non-linearity, high accuracy, and generalization capacity. Machine learning, capitalizing on extensive remote sensing data, has become pivotal in drought monitoring. By merging multi-source remote sensing data through machine learning models, the ground-based drought index can be replicated, expanding its spatial reach and offering a methodology to evaluate drought's spatial distribution. The Random Forest (RF) algorithm is a notable bagging integrated learning method. RF estimates rely on the average outcome of each tree within the forest, which helps prevent erratic prediction outcomes. Nevertheless, due to its averaging nature, RF might introduce bias when handling extreme data points. By implementing bias correction, the Bias-Corrected Random Forest (BRF) outperforms conventional RF models in extreme value estimation. XGBoost, an ensemble learning technique rooted in boosting, enhances gradient-augmented trees and serves as an efficient implementation of the Gradient Boosting Decision Tree (GBDT). Unlike RF, boosting generates results through a weighted aggregation of all predictions and is highly sensitive to anomalies. Support Vector Machine (SVM) stands as the closest machine learning approach to deep learning. Nonlinear SVM equates to a two-layer neural network. Introducing multiple kernel functions to nonlinear SVM can simulate a multi-layer neural network. Due to its robust classification and regression capabilities, SVM finds extensive applications in remote sensing and image classification.

## MATERIALS AND METHODS

**Study Areas:** The study was conducted in Shandong province, northern China, spanning approximately 157,900 km<sup>2</sup> with a water area of 2100 km<sup>2</sup>.

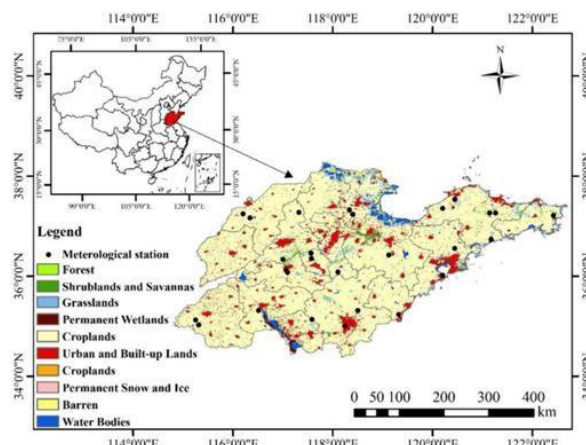


Figure 1: Study area: Shandong province's location and land cover types

Shandong's topography includes mountains, hills, platforms, basins, plains, lakes, and other features. It experiences a temperate monsoon climate, with annual precipitation ranging from 554 to 1048 mm. Precipitation decreases from southeast to north. Drought, mainly in spring and winter due to insufficient precipitation, affects winter wheat and summer maize, the primary crops. The survey used the IGBP land type classification standard in MCD12Q1 data to categorize Shandong's land use into various types, including forest, shrublands, grasslands, croplands, wetlands, urban areas, snow and ice, barren areas, and water bodies.

### Data

#### MODIS Data

The Moderate Resolution Imaging Spectroradiometer (MODIS) is a medium-resolution spectrometer situated on the Terra and Aqua satellites, playing a pivotal role in the U.S. Earth Observing System (EOS) program for monitoring global biological and physical phenomena. By capturing electromagnetic energy across a broad spectral range, MODIS delivers crucial insights into the Earth's ecological, meteorological, and hydrological dynamics. Throughout the research period spanning from 2002 to 2020, MODIS products, including the MCD12Q1 land cover type product, MOD13A3 vegetation index product, and MOD11A2 land surface temperature product, were acquired from NASA's official website (<http://reverb.echo.nasa.gov>, accessed on 12 February 2021).

Table 1: Remote Sensing Data used in this study

| Data          | Temporal Resolution | Spatial Resolution | Time Span | Source |
|---------------|---------------------|--------------------|-----------|--------|
| Precipitation | 1 month             | 0.1                | 2001-2020 | GPM    |

|                                     |                |             |                  |              |
|-------------------------------------|----------------|-------------|------------------|--------------|
| NDVI                                | 1 month        | 1 km        | 2002-2020        | MODIS        |
| EVI                                 | 1 month        | 1 km        | 2002-2020        | MODIS        |
| LST                                 | 8 day          | 1 km        | 2002-2020        | MODIS        |
| Soil moisture                       | 1 month        | 0.25        | 2002-2020        | MODIS        |
| Evapotranspiration                  | 1 month        | 0.25        | 2002-2020        | MODIS        |
| <u>Potential evapotranspiration</u> | <u>1 month</u> | <u>0.25</u> | <u>2002-2020</u> | <u>MODIS</u> |

MCD12Q1 characterizes land cover types annually at a spatial resolution of 500 m, while MOD13A3 synthesizes monthly surface vegetation index data at a 1 km resolution. Both NDVI and EVI data were utilized. MOD11A2, with an 8-day temporal resolution and 1 km spatial resolution, provides surface temperature information, aggregated into monthly values using the mean synthesis method [61]. All datasets were resampled to a spatial resolution of 500 m.

#### GPM Data

The Global Precipitation Measurement Mission (GPM) is an international collaboration led by NASA and JAXA, succeeding the Tropical Precipitation Measuring Mission (TRMM). GPM uses a core satellite with advanced radar/radiometer for space-based precipitation measurements. The GPM IMERG dataset, available on NASA's website, offers one-month temporal resolution and 0.1° spatial resolution (<https://search.earthdata.nasa.gov/>, accessed on February 17, 2021). To assess delayed precipitation response in drought conditions, we computed means for one-month and three-month scales, then resampled outcomes to a 500 m spatial resolution.

#### GLDAS Data

Data related to evapotranspiration, potential evapotranspiration, and soil moisture are derived from the GLDAS 2.1 (Global Land Data Assistance System Version 2.1) datasets. These datasets have monthly temporal resolution and a spatial resolution of 0.25° × 0.25°. GLDAS integrates satellite and ground measurements and employs advanced surface modeling and data assimilation techniques to estimate various surface states and fluxes continuously, including soil moisture, soil temperature, heat flux, and evaporation. The monthly soil moisture, potential evapotranspiration, and evapotranspiration data were originally obtained at a spatial resolution of 0.25° × 0.25° from the GLDAS-2.1 dataset and were later resampled to a spatial resolution of 500 m.

#### Observation Data

This research utilized meteorological data collected by the stations of the China Meteorological Data Network (<http://data.cma.cn/>, accessed on March 10, 2021). The data encompassed monthly precipitation, average temperature, and other metrics from Shandong meteorological stations spanning 2001 to 2020. The dataset included 23 meteorological stations, with their spatial arrangement depicted in Figure 1.

## A Method

### Modeling Methodology

This study outlines the agricultural drought assessment procedures, depicted in Figure 2, utilizing remote sensing data and model simulation data. The remote sensing drought factors, derived from multi-sensor remote sensing data, are employed to estimate the Standardized Precipitation Evapotranspiration Index (SPEI) using bias-corrected random forest (BRF), extreme gradient boosting (XGBoost), and support vector machines (SVM). These methods are applied to analyze drought conditions in Shandong province. *Maintaining the Integrity of the Specifications*

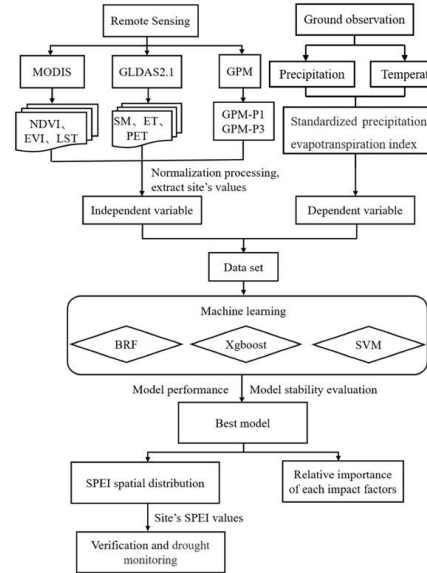


Figure 2: Workflow of this study

To begin, the drought index SPEI, based on meteorological station data (precipitation and temperature) from Shandong province, serves as the dependent variable for our model input. Next, remote sensing data are transformed into 500 m spatial resolution images using processes like projection coordinate conversion, resampling, band operation, and clipping via MRT, ArcGIS, and Python, incorporating maximum/minimum values. Three adaptive machine learning approaches—XGBoost, BRF, and SVM—are then applied to estimate agricultural drought in Shandong province using remote sensing drought factors. The selection of the best model is determined based on performance and stability evaluations

within the province. The relative importance of each influencing factor, as per the best model, is compared with the Pearson correlation coefficient of each factor with SPEI. Subsequently, the optimal drought monitoring model is utilized to generate the spatial distribution map of drought in Shandong province, with the SPEI spatial distribution map obtained through the model being analyzed for the province's drought situation.

**Standardized Precipitation Evapotranspiration Index**  
The SPEI, an extension of the SPI, combines precipitation and temperature for drought analysis [24]. Unlike SPI, SPEI considers temperature's impact on water needs. Shorter time scale SPEIs (e.g., SPEI-1) monitor meteorological drought, while longer ones are suitable for hydrological droughts. This study focuses on the three-month SPEI for monitoring agricultural and soil moisture dynamics.

The calculation steps of SPEI-3 are as follows:

1. Calculation of monthly potential evapotranspiration using Thornthwaite method:

$$PET = 16K(10T/I)^m \quad (1)$$

Equation (1), K represents the latitude-dependent correction factor, T denotes the monthly average temperature, I is the total heating index, and m stands for a constant

$$I = \sum_{i=1}^{12} I_i = 1(T/5)_{1.514} \quad (2)$$

$$m = 6.75 \times 10 - 7I_3 - 7.71 \times 10 - 5I_2 + 1.792 \times 10 - 2I + 0.49 \quad (3)$$

2. Calculate the difference between precipitation and potential evapotranspiration for each month

$$D_i = P_i - PET_i \quad (4)$$

Equation (4) defines  $P_i$  as the monthly precipitation,  $PET_i$  as the monthly potential evapotranspiration, and ' $i$ ' represents the month. The process of establishing the accumulation of climate water balance at various time scales follows.

$$Dkn = \sum_{i=1}^k D_i = 0(P_{n-i} - PET_{n-i}) \quad (5)$$

In Equation (5), the variable k represents the time scale and is assigned the numerical value of 3, while n denotes the quantity of computations.

3. To standardize  $D_i$ . Initially, a Log-logistic probability density function is employed to construct the dataset.

$$f(x) = \beta/\alpha(x-y/\alpha)^{\beta-1} [1+(x-y/\varepsilon)]^{-2} \quad (6)$$

In Equation (6),  $\alpha$  represents the scale parameter, and  $\beta$  signifies the shape parameter. These parameters are derived through the linear moment method. Subsequently, the cumulative probability of the  $D_i$  density function is expressed as:

$$F(x) = [1 + (\alpha/x - y)^{\beta}]^{-1} \quad (7)$$

4. Under normal normalization of the cumulative probability density function, the probability of exceeding a certain  $D_i$  value is  $P = 1 - F(X)$  and the probability of weighted moments are  $\omega = \sqrt{-2 \ln(P)}$ . When  $P \leq 0.5$ ,

$$SPEI = \omega - C_0 + C_1 \omega + C_2 \omega^2 / 1 + d_1 \omega + d_2 \omega^2 + d_3 \omega^3 \quad (8)$$

When  $P > 0.5$ ,

$$SPEI = C_0 + C_1 \omega + C_2 \omega^2 / 1 + d_1 \omega + d_2 \omega^2 + d_3 \omega^3 \quad (9)$$

In Equations (8) and (9),  $C_0 = 2.515517$ ,  $C_1 = 0.802853$ ,  $C_2 = 0.010328$ ,  $d_1 = 1.432788$ ,  $d_2 = 0.189269$ , and  $d_3 = 0.001308$

The temperature and precipitation records from chosen weather stations were employed to compute the standard precipitation evapotranspiration index (SPEI) based on ground observations. In accordance with globally accepted standards for categorizing drought severity, the SPEI is segmented into five levels, as outlined in Table 2.

**Table 2: SPEI-3 classification criteria for grading drought.**  
**Grade      Drought Condition      SPEI**

|     |                  |                    |
|-----|------------------|--------------------|
| I   | No Drought       | -0.5, SPEI         |
| II  | Light Drought    | -1.0 < SPEI < -0.5 |
| III | Moderate Drought | -1.5 < SPEI < 1.0  |
| IV  | Severe Drought   | -2.0 < SPEI < -1.5 |
| V   | Extreme Drought  | SPEI < -2.0        |

#### Establishment of Drought Prediction Indicators

This study calculated, the Soil Moisture Condition Index (SMCI) and Precipitation Condition Index (PCI) using soil moisture and precipitation data, respectively, both of which are closely associated with agricultural drought. PCI directly reflects deviations in precipitation, whereas SMCI provides a quantitative representation of soil moisture anomalies, indicating wet or dry conditions. The Temperature Condition Index (TCI) is derived from MODIS LST data and assesses the impact of high temperatures on vegetation growth; higher TCI values signify more severe drought conditions. Evapotranspiration indicates the level of plant transpiration, with lower values indicating greater drought severity. The calculation formulas are outlined in Table 3.

**Table 3: Normalization formula for calculating seven types of impact factors for each grid**

| Drought Index | Formula   |
|---------------|---|
| PCI           | $(GPM_1 - GPM_{min}) / (GPM_{max} - GPM_{min})$     |
| SMCI          | $(SM_1 - SM_{min}) / (SM_{max} - SM_{min})$         |
| TCI           | $(LST_{max} - LST_1) / (LST_{max} - LST_{min})$     |
| VCI           | $(NDVI_1 - NDVI_{min}) / (NDVI_{max} - NDVI_{min})$ |
| Scaled EVI    | $(EVI_1 - EVI_{min}) / (EVI_{max} - EVI_{min})$     |

|            |   |
|------------|---|
| Scaled ET  | $(ET_i - ET_{min}) / (ET_{max} - ET_{min})$     |
| Scaled PET | $(PET_i - PET_{min}) / (PET_{max} - PET_{min})$ |

Note: i represents the month; max and min represent the maximum and minimum values of the corresponding grid of the impact factor from 2002 to 2020.

### Bias-Corrected Random Forest

Random Forest (RF) is an integrated learning algorithm that constructs multiple decision trees into a random forest by random sampling and integration methods. RF first generates a number of independent trees using the sample set generated by bootstrap. With a large enough training sample, about 37% of the training data will be retained and used for subsequent out-of-bag validation. For each tree in the forest, RF determines its outcome by constructing a random subset of the training set through the bootstrap method. The result of RF approaches is the means of each tree. Therefore, RF can decrease the variance and obtain more precise prediction results compared with common tree-based algorithms. However, when predicting extreme observations, it may lead to bias. When the observations are small, the predictions of RF tend to overestimate; while when the observations are large, the predictions of RF tend to underestimate. In this study, we applied bias correction methods to estimate and correct for RF bias in the regression. The details of this bias-correction approach is as follows:

- 1) Firstly, build the RF model by training dataset  $Y_{train} = RF(X_{train})$ , where  $X_{train}$  and  $Y_{train}$  represent the independent and dependent variables, respectively.
- 2) Calculate the estimated value and residual,  $r_{train} = Y_{train} - Y_{predict}$ , where  $r_{train}$  represents the residual and  $Y_{predict}$  represents the estimated value.
- 3) Taking the residuals obtained in step (2) to be the dependent variable and training dataset in step (1) to be the independent variable, fit the random forest model,  $r_{train} = rfres(X_{train}, Y_{train})$ . This step is used to estimate the residual of the test dataset.
- 4) Calculate the estimated value  $Y_{test}$  from the RF model obtained in step (1) and the test dataset  $X_{test}$ ,  $Y_{test} = RF(X_{test})$
- 5) Calculate the estimated residual using the  $rfres$  model in step (3), the estimated value in step 4, and the independent variables in the test dataset,  $r_{test} = rfres(X_{test}, Y_{test})$
- 6) The estimated residual  $r_{test}$  is added to the estimated value  $Y_{test}$  for deviation correction,  $Y_{bias\text{-correction}} = Y_{test} + r_{test}$

### XGBoost

XGBoost, short for extreme gradient boosting, effectively implements the gradient boosting decision tree (GBDT) algorithm and incorporates numerous enhancements in both algorithmic and engineering aspects. In contrast to the conventional GBDT approach, XGBoost employs a data adoption strategy reminiscent of a random forest. Furthermore, it introduces a regularization term to manage model complexity, enhancing overall model generalization and preventing overfitting. The specifics of the XGBoost approach are outlined as follows.

- 1) To grow a tree, constantly add new trees and continuously split features. Each time a tree is added, a new function is learned  $f(x)$  to fit the residual of the last estimation. The optimal model is constructed by minimizing the loss function:  $obj(t) = \sum n \sum i=1 l(y_i, y_f) + \Omega(f(t)) + Constant$ .
- 2) XGBoost needs to estimate the result of a sample after it has been trained to obtain k trees. Actually, according to the characteristics of this sample, the sample will fall on one corresponding leaf node per tree, and each leaf node corresponds to a score.
- 3) Finally, XGBoost will add up the results corresponding to each tree, and it will obtain the estimate of the sample,  $y(k) = \sum K k y_k h_k(x_i)$ , where K is the sum of trees, k represents the kth tree,  $y_k$  is the weight of this tree, and  $h_k$  represents the estimation of this tree.

### Support Vector Machine

Support vector machine (SVM) is one of the most widely used algorithms in machine learning. Derived from statistical learning theory, SVM algorithms are strong learners with classification and regression algorithms. The purpose of SVM is to determine one or more hyperplanes to divide the samples. The segmentation principle is to maximize the interval, which is finally transformed into a convex quadratic programming problem. SVM is the closest machine learning method to deep learning. Nonlinear SVM is equivalent to a two-layer neural network. If multiple kernel functions are added to nonlinear SVM, a multi-layer neural network can be simulated. In this study, we implement the support vector regression model through Python's Scikit-learn machine learning library.

**Accuracy Evaluation** In this study, we enhance the machine learning approaches' performance by identifying the parameters that affect the models' stability through trial-and-error methods, and determine the optimal parameters for each model through cross validation. Then, BRF, XGBoost, and SVM are calibrated and validated with 80% and 20% of the dataset, respectively. The dataset is randomly sampled and divided into a training set and a test set. This step is performed 100 times to evaluate the stability of each model.

The

determination coefficient ( $R^2$ ) and mean square error ( $RMSE$ ) are used to evaluate the performance of the model:

$$R^2 = \left( \frac{\sum_{i=1}^n (O_i - \bar{O})(P_i - \bar{P})}{\sqrt{\sum_{i=1}^n (O_i - \bar{O})} \sqrt{\sum_{i=1}^n (P_i - \bar{P})}} \right)^2 \quad (10)$$

$$RMSE = \sqrt{\frac{\sum_{i=1}^n (O_i - P_i)^2}{n}} \quad (11)$$

where n is the number of samples,  $O_i$  and  $P_i$  are observed and estimated values, respectively, and  $\bar{O}$  and  $\bar{P}$  are the mean values of the observed and estimated values. Generally, the larger  $R^2$  and the smaller  $RMSE$ , the better the performance of the model is considered. In addition, we

performed station retention cross validation for each meteorological station to identify the stability of each model in the estimation of continuous time series of drought conditions.

## RESULTS

### Model Accuracy Comparison

This study trained BRF, XGBoost, and SVM models using selected influencing variables and observed SPEI-3 values. Following the determination of optimal parameters through cross-validation (as outlined in Table 4), we conducted a comparative analysis of the simulation accuracy of these algorithms. The findings indicate that the BRF model outperforms others in simulating SPEI-3 values, closely aligning simulated values with observed ones across each site month by month from 2002 to 2020 (refer to Figure 3). In both training and test sets, the determination coefficients ( $R^2$ ) for BRF fitting to SPEI-3 are 0.96 and 0.94, with root mean square errors ( $RMSE$ ) of 0.19 and 0.22, respectively. Notably, the bias-corrected approach significantly enhances the accuracy of random forests compared to prior studies, with BRF explaining over 90% of SPEI variation and exhibiting minimal prediction error. In contrast, SVM and XGBoost models demonstrate similar performance, each achieving  $R^2$  values of 0.72 and 0.74, along with  $RMSE$  values of 0.51 and 0.49, respectively.

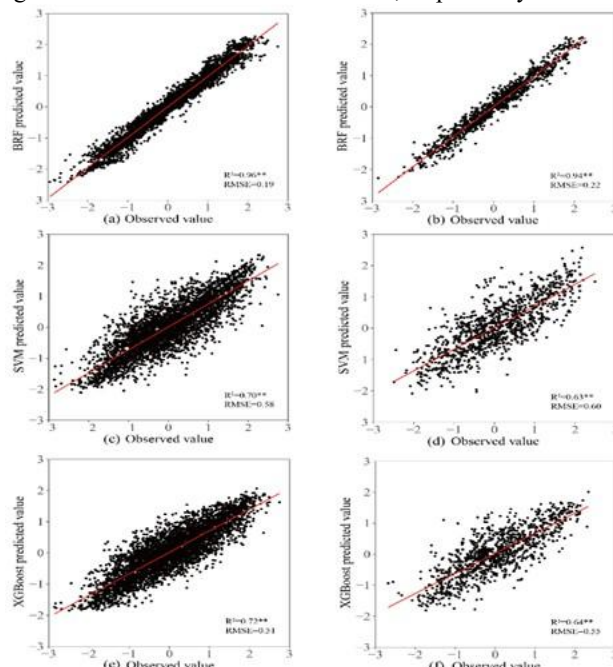


Figure 3: Scatterplot of model predictions vs. observations. (a,c,e) is the performance of BRF, SVM, and XGBoost on the training set. (b,d,f) is the performance of BRF, SVM, and XGBoost on the test set. “\*\*” represents the significance level of the experiment is greater than 0.99.

Table 4: The detailed list of parameters with their values used for BRF, XGBoost, and SVM.

| Model       | Parameters  |
|-------------|---|
| BRF         | RF1: criterion = ‘mse’, n_estimators = 800, max_depth = 5, min_samples_leaf=4,max_features=’auto’,random_state=0.bootstrap=true   |
| XGBo<br>ost | n_estimators=100, learning_rate=0.04, max_depth=5, gamma=0.5, consample_bytree=1,consample_bylevel=1,subsample=0.52,booster=’gbtree’,objective=’reg_squarederror’, reg_alpha=0.7,reg_lambda=0 |
| SVM         | Kernel=’rbf’,gamma=0.85,C=50,tol=0.01,cache_size=5000,dgree=3,coel0=2.5   |

## MODEL STABILITY EVALUATION

Randomly selected data sets were divided into calibration datasets and validation datasets. This step is performed 100 times to evaluate the stability of each model. The performance evaluation criteria ( $R^2$  and  $RMSE$ ) of the three models running 100 times are shown in Figure 4. Overall, based on these two validation measurements, the performance of the BRF model outperforms XGBoost and SVM, and the performance is satisfied. The BRF model explains more than 92% of the SPEI changes, and the estimation error is small ( $RMSE<0.25$ ). In comparison, the SVM and XGBoost models have similar and lower performance. Randomly selected data sets were divided into calibration datasets and validation datasets. This step is performed 100 times to evaluate the stability of each model. The performance evaluation criteria ( $R^2$  and  $RMSE$ ) of the three models running 100 times are shown in Figure 4. Overall, based on these two validation measurements, the performance of the BRF model outperforms XGBoost and SVM, and the performance is satisfied. The BRF model explains more than 92% of the SPEI changes, and the estimation error is small ( $RMSE<0.25$ ). In comparison, the SVM and XGBoost models have similar and lower performance.

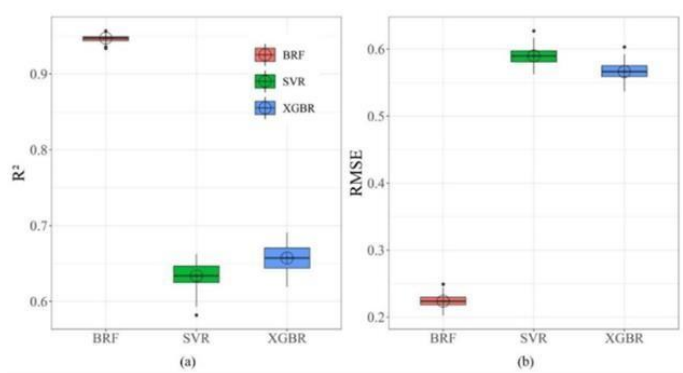


Figure 4: Boxplots of model performance measurements ((a). coefficient of determination and (b). root mean squared error) for prediction of SPEI.

To assess the model's stability further, we employed a "leave-one-station-out" cross-validation approach on the chosen 23 meteorological stations. Specifically, the meteorological stations in Heze, Huimin, Laiyang, and Yiyuan, situated in the eastern, western, southern, and northern regions of Shandong, respectively, were selected for this cross-validation. As depicted in Figure 5, the BRF model exhibited superior performance in off-site cross-validation, with the simulated drought conditions at the four stations generally aligning with SPEI-3 calculations based on observed data. In contrast, both SVM and XGBoost models performed less effectively than the BRF model, showing significant discrepancies in the simulated drought conditions compared to SPEI-3 calculations based on observed data at the four sites.

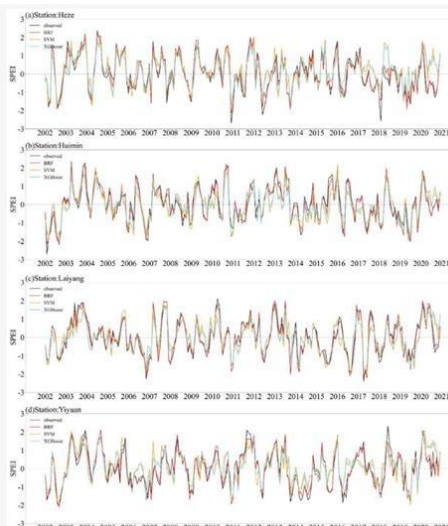


Figure 5: Comparation among SPEI-3 calculated from observations and forecasted by BRF, XGBoost, and SVM approaches at four stations in Shandong province, China.

#### Analyzing the Relative Importance of Drought-Influencing Factors Using the BRF Model

The BRF model can produce a measure of relative importance based on the impact of each predictor on the outcome. Table 5 displays the findings, revealing that Pre\_3 holds the highest relative importance at 55.17%. Notably, precipitation (Pre\_1) accounts for 8.61%, underscoring its pivotal role in drought impact. As we employed SPEI on a three-month time scale, SPEI-3 is linked to agricultural drought, emphasizing the heightened importance of cumulative precipitation in monitoring this type of drought. Soil moisture (SM) contributes significantly with a relative importance of 10.2%, highlighting its role in simulating agricultural drought. Conversely, the relative importance of other influencing factors remains low. Generally, the response of vegetation to drought is lagging, and the impact of drought on vegetation tends to occur after a few months, so this leads to a low relative importance of the vegetation indices NDVI and EVI.

Table 5: Relative importance of factors to drought assessment.

| <b>Impact Factors</b>                        | <b>Relative Importance (%)</b> |
|--|--------------------------------|
| One month Timescale precipitation, Pre_1     | 8.61                           |
| Three month Timescale precipitation, Pre_3   | 55.17                          |
| Land surface temperature, LST                | 7.39                           |
| Enhanced vegetation index, EVI               | 3.54                           |
| Normalized difference vegetation index, NDVI | 3.3                            |
| Soil moisture, SM                            | 10.2                           |
| Evapotranspiration, ET                       | 7.3                            |
| Potential evapotranspiration, PET            | 4.49                           |

We analyzed the correlation between SPEI-3 and drought impact factors, which are shown in Figure 6. The correlation analysis indicated that significant relationships existed among each factor and SPEI-3, with the highest correlation of 0.762 between PRE\_3 and SPEI-3. The correlations of SM and PRE\_1 with SPEI-3 were 0.55 and 0.449, respectively. The correlation between vegetation index and SPEI-3 was low. These were consistent with the results of our analysis of the relative importance of the factors obtained from the BRF model.



Figure 6: Pearson correlation coefficients of SPEI-3 with drought impact factors. The “1” and “3” suffixes following the variable name represent the average of one-month and three-month time scales.

#### Simulation of Drought by Spatial Distribution of SPEI-3 in Typical Years

In this research, the study utilized the average SPEI-3 values from 23 meteorological stations spanning the period from 2002 to 2020 to analyze the SPEI-3 change process. Figure 7 illustrates that significant and prolonged drought conditions were observed in 2002–2003, 2006–2007, and 2010–2011. Notably, severe drought occurred during the autumn of 2002 and 2006, winter of 2010, and spring of 2011. From 2012 to 2019, drought events were frequent but of low intensity. The years 2003–2004 and 2007–2008 marked wet periods across the entire province. However, there were no clear patterns regarding the duration and intensity of drought in other periods. The dashed box in Figure 7 highlights a specific period characterized by higher drought intensity and longer duration, selected as representative of typical drought years.

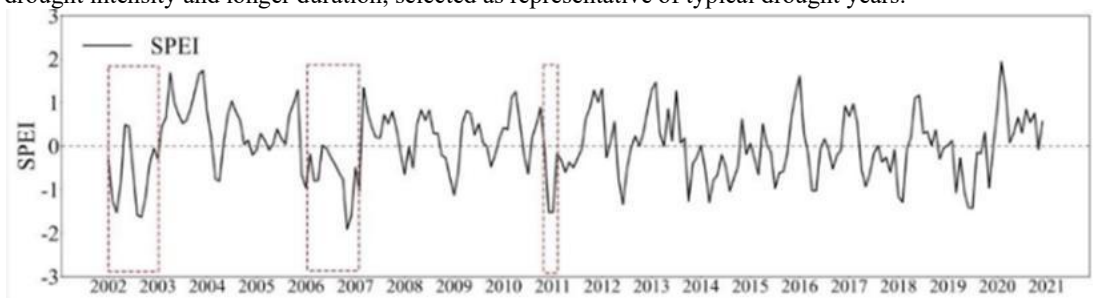


Figure 7: The change of SPEI-3 in Shandong province from 2002 to 2020.

The accuracy of SPEI-3 spatial distribution for drought monitoring was assessed using both SPEI-3 spatial distribution data and station observations of SPEI-3 data. Drought year data from 2002, 2006, and 2011 were specifically chosen for evaluation, and the corresponding results are illustrated in Figure 8, Figure 9, and Figure 10. Examining the drought grade distribution depicted in Figure 8 for meteorological stations, it is evident that all stations in northwestern Shandong province underwent severe drought in February. In contrast, other stations experienced varying degrees of moderate and light drought. March revealed a similar pattern, with most meteorological stations in western Shandong province facing severe drought, aligning well with the SPEI drought grade distribution map generated by BRF.

As the rain belt shifted southwest from April to June, drought conditions alleviated, and meteorological stations across the province were no longer experiencing drought. The summer of 2002 saw severe drought in Shandong due to high temperatures and low rainfall, affecting most stations except those in the eastern peninsula. This severe drought persisted from August to October, as reflected in the drought class distribution map created for this study. Ren and Zhan also monitored drought conditions in Shandong province during February–March and August–October 2002, highlighting increased severity from August to October. The occurrence of drought during this period in Shandong was linked to the El Niño phenomenon and prolonged absence of effective precipitation. In November, the drought dissipated with the subsiding high temperatures and the addition of effective precipitation.

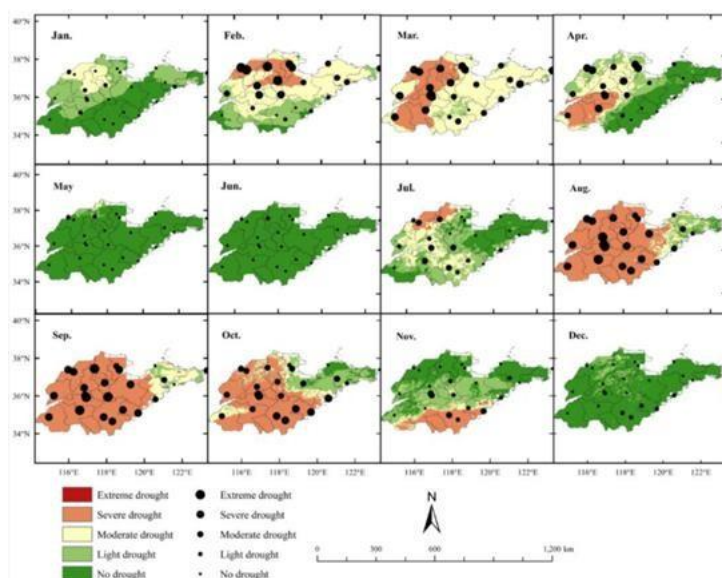


Figure 8: SPEI-3 spatial distribution simulated by the BRF model and the site's drought distribution in a drought year (2002)

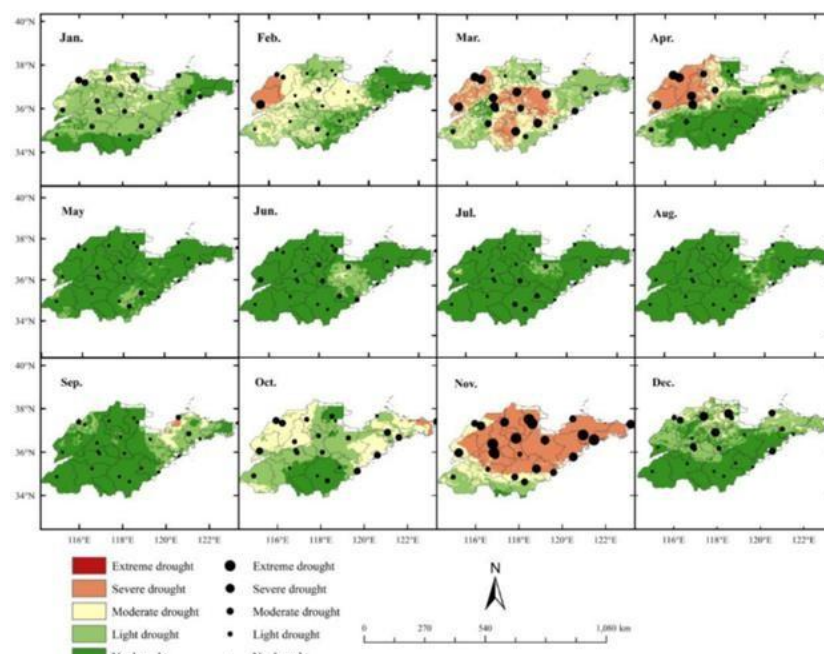
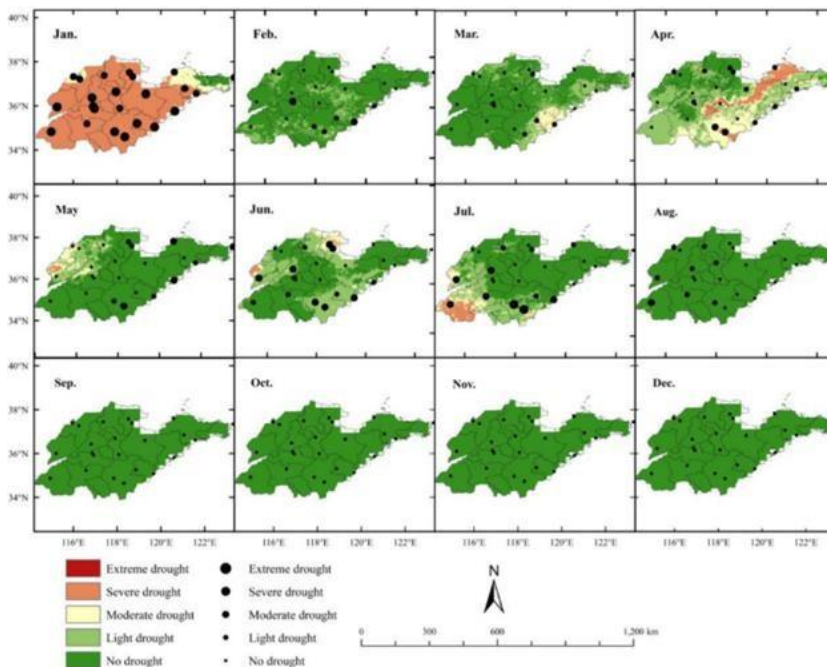


Figure 9: SPEI-3 spatial distribution simulated by the BRF model and the site's drought distribution in a drought year (2006).



*Figure 10: SPEI-3 spatial distribution simulated by the BRF model and the site's drought distribution in a drought year (2011).*

Figure 9 illustrates the drought conditions in Shandong province during different months. In January 2006, most meteorological stations experienced light drought, while some stations in the northwest faced moderate drought. In February, the eastern peninsula and southeast coast stations showed no drought or light drought, whereas the western part of Shandong had stations experiencing moderate and severe drought. In March, drought conditions intensified in the central and northwest regions, with meteorological stations detecting moderate and severe drought. April saw relief in the central part due to increased precipitation, but the northwest stations still endured severe drought. The arrival of the rainy season in May alleviated the overall drought in Shandong province. November witnessed severe and extreme drought at most stations, with some detecting moderate drought.

Figure 10 shows that in January 2011, all meteorological stations, except for some in the eastern peninsula, experienced severe and extreme drought, attributed to low precipitation from December 2010 to January 2011. The drought conditions align with the SPEI drought class distribution map. Yao et al. monitored the overall drought periods in Shandong province from February–March and November 2006, and December 2010–January 2011. In general, the BRF model's simulated SPEI-3 spatial distribution map accurately monitors drought conditions, consistent with historical drought studies' identified periods.

## DISCUSSION

Data-driven models, particularly the BRF model, proved effective in drought monitoring through machine learning with multi-source remote sensing factors fitting SPEI. BRF outperformed SVM and XGBoost, showcasing high  $R^2$  and low  $RMSE$ . However, Alizadeh and Nikoo found MLP significantly improved SPI prediction in Iran, differing from our results, possibly due to study area, data sources, and model variations. Model performance varied across regions, and BRF excelled due to reduced sensitivity to overfitting and handling hierarchical, nonlinear relationships between SPEI and remote sensing factors. Bias correction random forest surpassed the original random forest. The BRF model revealed precipitation on a three-month scale (GPM-P3) as the most crucial drought factor (55.17%), followed by GPM-P1 (8.61%). This aligns with Yang's findings on precipitation's significance in drought. GPM-P3's higher importance stems from SPEI's three-month scale selection, indicating its major impact on agricultural drought. Feng supported this, emphasizing the impact of three-month precipitation on agricultural drought. Soil moisture (SM) with 10.2% relative importance played a key role in simulating SPEI-3, consistent with Pearson correlation coefficients. GPM-P3 had the highest correlation (0.762) with SPEI-3, while SM's correlation was 0.55. SM-GPM-P3 (0.609) exceeded SM-GPM-P1 (0.526), indicating greater influence of cumulative precipitation on soil moisture. Using the BRF model and remote sensing data, we accurately predicted SPEI-3 in unmeasured areas without relying on relative importance as weights for a composite drought index. Constructing such an index based on weights often yields varying drought classifications across study areas, deviating from actual ground drought index distribution.

## CONCLUSION

In this research, the estimation of SPEI-3 in Shandong, China, employed three machine learning techniques (BRF, SVM, and XGBoost) alongside various factors influencing drought. The evaluation of SPEI predicted by the models was based on a monthly dataset derived from surface climate data. Notably, the BRF model successfully produced a spatial distribution map of SPEI-3, showcasing its applicability in regions with limited observation data and satellite coverage. Recognizing the multifaceted nature of drought, factors such as altitude and vegetation cover type were identified as influencers, emphasizing the necessity to incorporate them in future studies for enhanced model precision in drought monitoring. Despite the success, the BRF model exhibited limitations, notably a tendency to underestimate drought severity in extreme conditions.

Consequently, future research should explore advanced machine learning models and consider additional factors causing drought to enhance the models' performance, particularly in assessing extreme drought events.

## REFERENCES

- [1]. Ali, S.; Tong, D.M.; Xu, Z.T.; Henchiri, M.; Wilson, K.; Shi, S.Q.; Zhang, J.H. Characterization of Drought Monitoring Events through Modis-and Trmm-Based Dsi and TvdI over South Asia During 2001–2017. *Environ. Sci. Pollut. Res.* 2019, 26, 33568–33581.
- [2]. Quiring, S.M.; Papakryiakou, T.N. An Evaluation of Agricultural Drought Indices for the Canadian Prairies. *Agric. For. Meteorol.* 2003, 118, 49–62.
- [3]. Wei, W.; Pang, S.F.; Wang, X.F.; Zhou, L.; Xie, B.B.; Zhou, J.J.; Li, C.H. Temperature Vegetation Precipitation Dryness Index (Tvpdi)-Based Dryness-Wetness Monitoring in China. *Remote Sens. Environ.* 2020, 248, 111957.
- [4]. Yao, N.; Li, Y.; Lei, T.J.; Peng, L.L. Drought Evolution, Severity and Trends in Mainland China over 1961–2013. *Sci. Total Environ.* 2018, 616, 73–89.
- [5]. Trenberth, K.E.; Dai, A.; Van Der Schrier, G.; Jones, P.D.; Barichivich, J.; Briffa, K.R.; Sheffield, J. Global Warming and Changes in Drought. *Nat. Clim. Change* 2014, 4, 17.
- [6]. Dai, A.G. Erratum: Drought under Global Warming: A Review. *Wiley Interdiscip. Rev.-Clim. Chang.* 2012, 3, 617.
- [7]. Vicente-Serrano, S.M.; Quiring, S.M.; Pena-Gallardo, M.; Yuan, S.S.; Dominguez-Castro, F. A Review of Environmental Droughts: Increased Risk under Global Warming? *Earth-Sci. Rev.* 2020, 201, 102953.
- [8]. Daryanto, S.; Wang, L.X.; Jacinthe, P.A. Global Synthesis of Drought Effects on Food Legume Production. *PLoS ONE* 2015, 10, e0127401.
- [9]. Daryanto, S.; Wang, L.X.; Jacinthe, P.A. Global Synthesis of Drought Effects on Maize and Wheat Production. *PLoS ONE* 2016, 11, e0156362.
- [10]. Loon, V.; Anne, F. Hydrological Drought Explained. *Wiley Interdiscip. Rev. Water* 2015, 2, 359–392.
- [11]. Allen, C.D.; Macalady, A.K.; Chenchouni, H.; Bachelet, D.; McDowell, N.; Vennetier, M.; Kitzberger, T.; Rigling, A.; Breshears, D.D.; Hogg, E.H.; et al. A Global Overview of Drought and Heat-Induced Tree Mortality Reveals Emerging Climate Change Risks for Forests. *For. Ecol. Manag.* 2010, 259, 660–684.
- [12]. Ciais, P.; Reichstein, M.; Viovy, N.; Granier, A.; Ogee, J.; Allard, V.; Aubinet, M.; Buchmann, N.; Bernhofer, C.; Carrara, A.; et al. Europe-Wide Reduction in Primary Productivity Caused by the Heat and Drought in 2003. *Nature* 2005, 437, 529–533.
- [13]. Zhao, M.S.; Running, S.W. Drought-Induced Reduction in Global Terrestrial Net Primary Production from 2000 through 2009. *Science* 2010, 329, 940–943.
- [14]. Aadhar, S.; Mishra, V. High-Resolution near Real-Time Drought Monitoring in South Asia. *Sci. Data* 2017, 4, 170145.
- [15]. He, B.; Wu, J.J.; Lu, A.F.; Cui, X.F.; Zhou, L.; Liu, M.; Zhao, L. Quantitative Assessment and Spatial Characteristic Analysis of Agricultural Drought Risk in China. *Nat. Hazards* 2013, 66, 155–166.
- [16]. Mottaleb, K.A.; Gumma, M.K.; Mishra, A.K.; Mohanty, S. Quantifying Production Losses Due to Drought and Submergence of Rainfed Rice at the Household Level Using Remotely Sensed Modis Data. *Agric. Syst.* 2015, 137, 227–235.
- [17]. Prodhan, F.A.; Zhang, J.H.; Yao, F.M.; Shi, L.M.; Sharma, T.P.P.; Zhang, D.; Cao, D.; Zheng, M.X.; Ahmed, N.; Mohana, H.P. Deep Learning for Monitoring Agricultural Drought in South Asia Using Remote Sensing Data. *Remote Sens.* 2021, 13, 1715.
- [18]. Yang, X.; Li, D. Temporal and Spatial Evolution Characteristics of Strong Drought Events in North and Northeast China. *Arid Land Geogr.* 2019, 42, 810–821.
- [19]. Ren, J.; Zhang, T. Evolution Characteristics of Drought and Flood in Shandong Province in Recent 45years Based on Standardized Precipitation Index. *Res. Soil Water Conserv.* 2021, 28, 149.
- [20]. Zhang, J.; Mu, Q.Z.; Huang, J.X. Assessing the Remotely Sensed Drought Severity Index for Agricultural Drought Monitoring and Impact Analysis in North China. *Ecol. Indic.* 2016, 63, 296–309.
- [21]. Yan, H.; Wan, Y.; Yan, X.; Xie, Y. A Study of the Temporal and Spatial Features of Dryness & Wetness Last 500Year Period in China. *J. Yunnan Univ. (Nat. Sci.)* 2004, 26, 139–143.
- [22]. Zhang, Y.; Wang, C.; Zhang, J. Analysis of the Spatial and Temporal Characteristics of Drought in the North China Plain Based on Standardized Precipitation Evapotranspiration Index. *Acta Ecol. Sin.* 2015, 35, 7097–7107.
- [23]. McKee, T.B.; Doesken, N.J.; Kleist, J. The Relationship of Drought Frequency and Duration to Time Scales. In Proceedings of the 8th Conference on Applied Climatology, Anaheim, CA, USA, 17–22 January 1993; pp. 179–184.
- [24]. Feng, P.Y.; Wang, B.; Liu, D.L.; Yu, Q. Machine Learning-Based Integration of Remotely-Sensed Drought Factors Can Improve the Estimation of Agricultural Drought in South-Eastern Australia. *Agric. Syst.* 2019, 173, 303–316.
- [25]. Rhee, J.; Im, J.; Carbone, G.J. Monitoring Agricultural Drought for Arid and Humid Regions Using Multi-Sensor Remote Sensing Data. *Remote Sens. Environ.* 2010, 114, 2875–2887.

- [26]. Liu, Q.; Zhang, J.H.; Zhang, H.R.; Yao, F.M.; Bai, Y.; Zhang, S.; Meng, X.L.; Liu, Q. Evaluating the Performance of Eight Drought Indices for Capturing Soil Moisture Dynamics in Various Vegetation Regions over China. *Sci. Total Environ.* 2021, **789**, 147803.
- [27]. Yao, N.; Li, Y.; Liu, Q.Z.; Zhang, S.Y.; Chen, X.G.; Ji, Y.D.; Liu, F.G.; Pulatov, A.; Feng, P.Y. Response of Wheat and Maize Growth-Yields to Meteorological and Agricultural Droughts Based on Standardized Precipitation Evapotranspiration Indexes and Soil Moisture Deficit Indexes. *Agric. Water Manag.* 2022, **266**, 107566.
- [28]. Swain, S.; Wardlow, B.D.; Narumalani, S.; Tadesse, T.; Callahan, K. Assessment of Vegetation Response to Drought in Nebraska Using Terra-Modis Land Surface Temperature and Normalized Difference Vegetation Index. *Giscience Remote Sens.* 2011, **48**, 432–455.
- [29]. Ali, S.; Henchiri, M.; Yao, F.M.; Zhang, J.H. Analysis of Vegetation Dynamics, Drought in Relation with Climate over South Asia from 1990 to 2011. *Environ. Sci. Pollut. Res.* 2019, **26**, 11470–11481.
- [30]. Shi, S.Q.; Yao, F.M.; Zhang, J.H.; Yang, S.S. Evaluation of Temperature Vegetation Dryness Index on Drought Monitoring over Eurasia. *IEEE Access* 2020, **8**, 30050–30059.
- [31]. Wu, D.; Qu, J.J.; Hao, X.J. Agricultural Drought Monitoring Using Modis-Based Drought Indices over the USA Corn Belt. *Int. J. Remote Sens.* 2015, **36**, 5403–5425.
- [32]. Souza, A.; Neto, A.R.; Rossato, L.; Alvala, R.C.S.; Souza, L.L. Use of Smos L3 Soil Moisture Data: Validation and Drought Assessment for Pernambuco State, Northeast Brazil. *Remote Sens.* 2018, **10**, 1314.
- [33]. Bai, Y.; Gao, J.; Zhang, B. Monitoring of Crops Growth Based on Ndvi and Evi. *Trans. Chin. Soc. Agric. Mach.* 2019, **50**, 153–161.
- [34]. Gu, Y.X.; Brown, J.F.; Verdin, J.P.; Wardlow, B. A Five-Year Analysis of Modis Ndvi and Ndwi for Grassland Drought Assessment over the Central Great Plains of the United States. *Geophys. Res. Lett.* 2007, **34**.
- [35]. Lei, Q.; Zhang, X.; Wang, X.; He, X.; Shang, C. Responses of Vegetation Index to Meteorological Drought in Dongting Lake Basin Based on Modis-Evi and Ci. *Resour. Environ. Yangtze Basin* 2019, **28**, 981–993.
- [36]. Wang, K.Y.; Li, T.J.; Wei, J.H. Exploring Drought Conditions in the Three River Headwaters Region from 2002 to 2011 Using Multiple Drought Indices. *Water* 2019, **11**, 190.
- [37]. Liu, H.; Liu, R.; Liu, S. Review of Drought Monitoring by Remote Sensing. *J. Geo-Inf. Sci.* 2012, **14**, 232–239.
- [38]. Alizadeh, M.R.; Nikoo, M.R. A Fusion-Based Methodology for Meteorological Drought Estimation Using Remote Sensing Data. *Remote Sens. Environ.* 2018, **211**, 229–247.
- [39]. Han, P.; Wang, P.X.; Zhang, S.Y.; Zhu, D.H. Drought Forecasting Based on the Remote Sensing Data Using Arima Models. *Math. Comput. Model.* 2010, **51**, 1398–1403.
- [40]. Mishra, A.K.; Singh, V.P. Drought Modeling—A Review. *J. Hydrol.* 2011, **403**, 157–175.
- [41]. Swain, S.; Wardlow, B.D.; Narumalani, S.; Tadesse, T.; Callahan, K. Assessment of Vegetation Response to Drought in Nebraska Using Terra-Modis Land Surface Temperature and Normalized Difference Vegetation Index. *Giscience Remote Sens.* 2011, **48**, 432–455.
- [42]. Park, S.; Im, J.; Jang, E.; Rhee, J. Drought Assessment and Monitoring through Blending of Multi-Sensor Indices Using Machine Learning Approaches for Different Climate Regions. *Agric. For. Meteorol.* 2016, **216**, 157–169.
- [43]. Mishra, A.K.; Singh, V.P. Drought Modeling—A Review. *J. Hydrol.* 2011, **403**, 157–175.
- [44]. Wanders, N.; Wood, E.F. Improved Sub-Seasonal Meteorological Forecast Skill Using Weighted Multi-Model Ensemble Simulations. *Environ. Res. Lett.* 2016, **11**, 094007.
- [45]. Morid, S.; Smakhtin, V.; Bagherzadeh, K. Drought Forecasting Using Artificial Neural Networks and Time Series of Drought Indices. *Int. J. Climatol.* 2007, **27**, 2103–2111.
- [46]. Wang, Q.J.; Schepen, A.; Robertson, D.E. Merging Seasonal Rainfall Forecasts from Multiple Statistical Models through Bayesian Model Averaging. *J. Clim.* 2012, **25**, 5524–5537.
- [47]. Abbot, J.; Marohasy, J. Input Selection and Optimisation for Monthly Rainfall Forecasting in Queensland, Australia, Using Artificial Neural Networks. *Atmos. Res.* 2014, **138**, 166–178.
- [48]. Hao, Z.C.; Singh, V.P.; Xia, Y.L. Seasonal Drought Prediction: Advances, Challenges, and Future Prospects. *Rev. Geophys.* 2018, **56**, 108–141.
- [49]. Barua, S.; Ng, A.W.M.; Perera, B.J.C. Artificial Neural Network-Based Drought Forecasting Using a Nonlinear Aggregated Drought Index. *J. Hydrol. Eng.* 2012, **17**, 1408–1413.
- [50]. Dikshit, A.; Pradhan, B.; Alamri, A.M. Temporal Hydrological Drought Index Forecasting for New South Wales, Australia Using Machine Learning Approaches. *Atmosphere* 2020, **11**, 585.
- [51]. Khan, N.; Sachindra, D.A.; Shahid, S.; Ahmed, K.; Shiru, M.S.; Nawaz, N. Prediction of Droughts over Pakistan Using Machine Learning Algorithms. *Adv. Water Resour.* 2020, **139**, 103562.
- [52]. Belayneh, A.; Adamowski, J.; Khalil, B.; Ozga-Zielinski, B. Long-Term Spi Drought Forecasting in the Awash River Basin in Ethiopia Using Wavelet Neural Network and Wavelet Support Vector Regression Models. *J. Hydrol.* 2014, **508**, 418–429.
- [53]. Guzman, S.M.; Paz, J.O.; Tagert, M.L.M.; Mercer, A.E.; Pote, J.W. An Integrated Svr and Crop Model to Estimate the Impacts of Irrigation on Daily Groundwater Levels. *Agric. Syst.* 2018, **159**, 248–259.
- [54]. Cutler, D.R.; Edwards, T.C.; Beard, K.H.; Cutler, A.; Hess, K.T.; Gibson, J.; Lawler, J.J. Random Forests for Classification in Ecology. *Ecology* 2007, **88**, 2783–2792.

- [55]. Song, J. Bias Corrections for Random Forest in Regression Using Residual Rotation. *J. Korean Stat. Soc.* 2015, 44, 321–326.
- [56]. Chen, T.Q.; Guestrin, C.; Assoc Comp, M. Xgboost: A Scalable Tree Boosting System. In Proceedings of the 22nd ACM SIGKDD International Conference on Knowledge Discovery and Data Mining (KDD), San Francisco, CA, USA, 13–17 August 2016.
- [57]. Chen, Y.; Niu, J.Q.; Chen, G.Q.; Wang, J.; Cao, S.L.; Publishing, I.O.P. Precipitation Sequence Analysis of Representative Stations in Shandong Province from 1956 to 2016. In Proceedings of the 6th International Conference on Energy Materials and Environment Engineering (ICEMEE), Zhangjiajie, China, 24–26 April 2020.
- [58]. Li, H.; Wang, W. Climate Characteristics of Seasonal Drought for Crops Growth in Shandong. *J. Arid Land Resour. Environ.* 2015, 29, 191–196.
- [59]. Li, F.; Yang, X. Changes and Driving Force of Grain Production in Shandong Province During 1999–2014. *Acta Agric. Zhejiangensis* 2016, 28, 535–542.
- [60]. Han, H.Z.; Bai, J.J.; Yan, J.W.; Yang, H.Y.; Ma, G. A Combined Drought Monitoring Index Based on MultiSensor Remote Sensing Data and Machine Learning. *Geocarto Int.* 2021, 36, 1161–1177.
- [61]. Shen, R.P.; Huang, A.Q.; Li, B.L.; Guo, J. Construction of a Drought Monitoring Model Using Deep Learning Based on Multi-Source Remote Sensing Data. *Int. J. Appl. Earth Obs. Geoinf.* 2019, 79, 48–57.
- [62]. Tapiador, F.J.; Turk, F.J.; Petersen, W.; Hou, A.Y.; Garcia-Ortega, E.; Machado, L.A.; Angelis, C.F.; Salio, P.; Kidd, C.; Huffman, G.J.; et al. Global Precipitation Measurement: Methods, Datasets and Applications. *Atmos. Res.* 2012, 104, 70–97.
- [63]. Zhao, J.; Yan, D.H.; Yang, Z.Y.; Hu, Y.; Weng, B.S.; Gong, B.Y. Improvement and Adaptability Evaluation of Standardized Precipitation Evapotranspiration Index. *Acta Phys. Sin.* 2015, 64, 049202.
- [64]. Almeida-Naunay, A.F.; Villeta, M.; Quemada, M.; Tarquis, A.M. Assessment of Drought Indexes on Different Time Scales: A Case in Semiarid Mediterranean Grasslands. *Remote Sens.* 2022, 14, 565.
- [65]. Wen, J.; Zhang, X.; Wang, Y.; Wang, W. Effects of Drought in Multi-Time Scale on Wheat Crop in Eastern Agricultural Region of Qinghai Province. *J. Irrig. Drain.* 2016, 35, 92–97.
- [66]. Javed, T.; Zhang, J.H.; Bhattacharai, N.; Sha, Z.; Rashid, S.; Yun, B.; Ahmad, S.; Henchiri, M.; Kamran, M. Drought Characterization across Agricultural Regions of China Using Standardized Precipitation and Vegetation Water Supply Indices. *J. Clean. Prod.* 2021, 313,
- [67]. Zhang, J.H.; Zhou, Z.M.; Yao, F.M.; Yang, L.M.; Hao, C. Validating the Modified Perpendicular Drought Index in the North China Region Using in Situ Soil Moisture Measurement. *IEEE Geosci. Remote Sens. Lett.* 2015, 12, 542–546.
- [68]. Wu, L. Classification of Drought Grades Based on Temperature Vegetation Drought Index Using the Modis Data. *Res. Soil Water Conserv.* 2017, 24, 130–135.
- [69]. Wang, Y.P.; Wang, S.; Zhao, W.W.; Liu, Y.X. The Increasing Contribution of Potential Evapotranspiration to Severe Droughts in the Yellow River Basin. *J. Hydrol.* 2022, 605, 127310.
- [70]. Seiler, R.A.; Kogan, F.; Sullivan, J. Avhrr-Based Vegetation and Temperature Condition Indices for Drought Detection in Argentina. *Adv. Space Res.* 1998, 21, 481–484.
- [71]. Kogan, F.N. Application of Vegetation Index and Brightness Temperature for Drought Detection. *Adv. Space Res.* 1995, 15, 91–100.
- [72]. Ishwaran, H.; Malley, J.D. Synthetic Learning Machines. *Biodata Min.* 2014, 7, 28.
- [73]. Zhang, G.Y.; Lu, Y. Bias-Corrected Random Forests in Regression. *J. Appl. Stat.* 2012, 39, 151–160.
- [74]. Li, H.; Zhu, Y. Xgboost Algorithm Optimization Based on Gradient Distribution Harmonized Strategy. *J. Comput. Appl.* 2020, 40, 1633–1637.
- [75]. Chen, J.X.; Zhao, F.; Sun, Y.G.; Yin, Y.L. Improved Xgboost Model Based on Genetic Algorithm. *Int. J. Comput. Appl. Technol.* 2020, 62, 240–245.
- [76]. Corinna, C.; Vladimir, V. Support-Vector Networks. *Mach. Learn.* 1995, 20, 273–297.
- [77]. Haitao, L.I.; Haiyan, G.U.; Bing, Z.; Lianru, G. Research on Hyperspectral Remote Sensing Image Classification Based on Mnf and Svm. *Remote Sens. Inf.* 2007, 5, 12–15.
- [78]. Mountrakis, G.; Im, J.; Ogole, C. Support Vector Machines in Remote Sensing: A Review. *Isprs J. Photogramm. Remote Sens.* 2011, 66, 247–259.
- [79]. Shen, R.; Guo, J.; Zhang, J.; Li, L. Construction of a Drought Monitoring Model Using the Random Forest Based Remote Sensing. *J. Geo-Inf. Sci.* 2017, 19, 125–133.
- [80]. Were, K.; Bui, D.T.; Dick, O.B.; Singh, B.R. A Comparative Assessment of Support Vector Regression, Artificial Neural Networks, and Random Forests for Predicting and Mapping Soil Organic Carbon Stocks across an Afromontane Landscape. *Ecol. Indic.* 2015, 52, 394–403.
- [81]. Xu, Z.; Han, M. Spatio-Temporal Distribution Characteristics of Drought in Shandong Province and Its Relationship with Enso. *Chin. J. Eco-Agric.* 2018, 26, 1236–1248.
- [82]. Yao, T.; Zhao, Q.; Li, X.Y.; Shen, Z.T.; Ran, P.Y.; Wu, W. Spatiotemporal Variations of Multi-Scale Drought in Shandong Province from 1961 to 2017. *Water Supply* 2021, 21, 525–541.

- [83]. Yang, M.X.; Mou, Y.L.; Meng, Y.R.; Liu, S.; Peng, C.H.; Zhou, X.L. Modeling the Effects of Precipitation and Temperature Patterns on Agricultural Drought in China from 1949 to 2015. *Sci. Total Environ.* 2020, 711, 135139.
- [84]. Seneviratne, S.I.; Corti, T.; Davin, E.L.; Hirschi, M.; Jaeger, E.B.; Lehner, I.; Orlowsky, B.; Teuling, A.J. Investigating Soil Moisture-Climate Interactions in a Changing Climate: A Review. *Earth-Sci. Rev.* 2010, 99, 125–161.
- [85]. Sims, A.P.; Niyogi, D.D.S.; Raman, S. Adopting Drought Indices for Estimating Soil Moisture: A North Carolina Case Study. *Geophys. Res. Lett.* 2002, 29, 24-1–24-4.